SAND REPORT

SAND2001-3522
Unlimited Release
Printed November 2001

Distributed Sensor Particles for Remote Fluorescence Detection of Trace Analytes: UXO/CW

Anup K Singh, Alok Gupta, Ashok Mulchandani, Wilfred Chen, Rimple B. Bhatia, Joseph S. Schoeniger, Carol S. Ashley, C. Jeffrey Brinker, Bradley G. Hance, Randal L. Schmitt, Mark S. Johnson, Philip J. Hargis, Jr., and R. Joseph Simonson

Prepared by
Sandia National Laboratories
Albuquerque, New Mexico 87185 and Livermore, California 94550

Sandia is a multiprogram laboratory operated by Sandia Corporation, a Lockheed Martin Company, for the United States Department of Energy under Contract DE-AC04-94AL85000.

Issued by Sandia National Laboratories, operated for the
United States Department of Energy by Sandia Corporation.

Available to DOE and DOE contractors from
U.S. Department of Energy
Office of Scientific and Technical Information
P.O. Box 62
Oak Ridge, TN 37831

Telephone: (865)576-8401
Facsimile: (865)576-5728
E-Mail: reports@adonis.osti.gov
Online ordering: http://www.doe.gov/bridge

Available to the public from
U.S. Department of Commerce
National Technical Information Service
5285 Port Royal Rd
Springfield, VA 22161

Telephone: (800)553-6847
Facsimile: (703)605-6900
E-Mail: orders@ntis.fedworld.gov
Online order: http://www.ntis.gov/ordering.htm

SAND2001-3522
Unlimited Release
Printed November 2001

Distributed Sensor Particles for Remote Fluorescence Detection of Trace Analytes: UXO/CW

Anup K Singh[a], Alok Gupta[a], Ashok Mulchandani[b], Wilfred Chen[b], Rimple B. Bhatia[c], Joseph S. Schoeniger[a], Carol S. Ashley[d], C. Jeffrey Brinker[c,d], Bradley G. Hance[d], Randal L. Schmitt[d], Mark S. Johnson[d], Philip J. Hargis, Jr.[d],
and R. Joseph Simonson[d*]

[a]Sandia National Laboratory, Livermore, CA 94551-0969
[b]Dept. of Chemical and Environmental Engineering, Univ. of California, Riverside, CA
[c]Univ. of New Mexico/Center for Microengineered Materials, Albuquerque, NM 87106
[d]Sandia National Laboratory, Albuquerque, NM 87185

Abstract follows

* Author to whom correspondence should be addressed: rjsimon@sandia.gov

Abstract

This report summarizes the development of sensor particles for remote detection of trace chemical analytes over broad areas, e.g residual trinitrotoluene from buried landmines or other unexploded ordnance (UXO). We also describe the potential of the sensor particle approach for the detection of chemical warfare (CW) agents. The primary goal of this work has been the development of sensor particles that incorporate sample preconcentration, analyte molecular recognition, chemical signal amplification, and fluorescence signal transduction within a "grain of sand". Two approaches for particle-based chemical-to-fluorescence signal transduction are described: (1) enzyme-amplified immunoassays using biocompatible inorganic encapsulants, and (2) oxidative quenching of a unique fluorescent polymer by TNT.

Acknowledgements

This work was supported by the Laboratory Directed Research and Development program at Sandia National Laboratories.

Contents

Figures

Tables

1. Introduction

The goal of the work described in this report is the development of sensor particles for remote detection of trace chemical analytes over broad areas. Since the original purpose of this research was the detection of buried landmines or other unexploded ordnance (UXO), much of the work is directed toward the detection of trinitrotoluene, the explosive used in a majority of landmines. We have also investigated the potential of the sensor particle approach for the detection of chemical warfare (CW) agents.

Consideration of remote optical detection requirements led to fluorescence emission as the most promising candidate technique for interrogation of the chemical sensor particles. Therefore, the primary goal of this work has been the development of sensor particles that incorporate sample preconcentration, analyte molecular recognition, chemical signal amplification, and fluorescence signal transduction within a "grain of sand". In a deployment scenario such granular sensors could be distributed over areas of interest using "crop duster" aircraft. The fluorescent signature produced by the ensemble of dispersed sensors can be detected by remote standoff fluorescence Light Detection and Ranging (LIDAR) systems. This could in turn potentially enable land mine mapping or CW agent detection without direct sample collection from the position(s) of interest. To successfully implement this detection scheme we must overcome several difficult problems. The expected analyte target concentrations relevant for the CW and UXO detection problems are small (ppm range or less), subject to environmental variation, and difficult to quantify. Thus to achieve useful signal/noise for optical remote sensing of such chemical targets, we assume that the detection chemistry must be highly specific, must incorporate significant chemical amplification, and must result in the production of fluorescence signatures with high fluorescent efficiencies and favorable excitation and emission maxima.

To date, we have investigated two approaches for particle-based chemical-to-fluorescence signal transduction. The first relies on enzyme-amplified immunoassays, with the necessary biomolecules immobilized within the pores of a sol-gel synthesized inorganic host matrix. We have successfully demonstrated this concept by developing a TNT enzyme-amplified immunoassay within a silica host matrix. In addition, complete cells have been immobilized in such hosts, with potential usefulness in CW detection applications. The details of this work are summarized in Sections 2 and 3 of this report. Section 4 describes efforts to produce modified enzymes for use in this detection approach. Modification of the enzymes has the potential both to increase the sensitivity of this detection scheme, and to enable use of this approach for detection of a broad range of target analytes.

The second transduction mechanism we investigated for remote particle-based sensing relies on oxidative quenching of a unique fluorescent polymer by TNT. This method is significantly simpler to implement than the immunoassay approach, but is not as readily adapted to detection of chemical targets other than nitroaromatic explosives. Using this approach, we have successfully demonstrated the detection of ~ 1 ppm of TNT in natural soil at a standoff range of 0.5 km. These results are described in Section 6.

Section 5 of this report summarizes estimates of fluorescence signal to noise (SNR) for remote detection of sensor particles using notional imaging and non-imaging LIDAR systems, based on a simple spreadsheet model.

2. Aqueous sol-gel process for protein encapsulation

Abstract

Porous silica materials made by low temperature sol-gel process are promising host matrixes for encapsulation of biomolecules. To date, researchers have focussed on sol-gel routes using alkoxides such as tetramethyl orthosilicate (TMOS) and tetraethyl orthosilicate (TEOS) for encapsulation of biomolecules. These routes lead to formation of alcohol as a byproduct that can have detrimental effect on the activity of entrapped biomolecules. We have developed a novel aqueous sol-gel process to encapsulate biological molecules (such as enzymes, antibodies and cells) that uses neutral pH, room temperature, and does not generate alcohol as a byproduct. The process uses sodium silicate as precursor and is carried out in two steps- preparation of a low pH silicate sol followed by gelation at neutral pH with a suitable buffer containing biomolecules. Two enzymes widely used in biosensing applications- horseradish peroxidase (HRP) and glucose-6-phosphate dehydrogenase (G6PDH), were used to prepare enzyme-doped silica monoliths and to investigate the effect of silica as host matrix on enzyme kinetics. The yield of encapsulation process was about 100% for both enzymes and no significant leaching of enzyme molecules was observed over time. Encapsulated enzymes followed Michaelis-Menten kinetics and maintained good catalytic activity; the specific activity of encapsulated HRP and G6PDH being 73% and 36% of the specific activities of free enzymes, respectively. The values of Michaelis'constant (K_m) of the encapsulated enzymes were higher than those of the free enzymes, indicating the presence of partitioning and diffusional effects in the pores of sol-gel matrix. The encapsulated enzymes also exhibited a different pH dependence of catalytic activity; the pH maxima for enzymatic activity for encapsulated enzymes were higher by 0.5-1 pH unit than those for enzymes in solution. These novel enzyme-doped silica matrixes provide promising platforms for development of biosensors, affinity supports, and immobilized enzyme reactors.

Aqueous Sol-Gel Process for Protein Encapsulation
Rimple Bhatia, C. Jeffrey Brinker, Alok Gupta and Anup Singh
Chemistry of Materials 12(8) (2000), 2434-2441

3. Encapsulation of enzymes and cells in sol-gel matrices for biosensor applications

Abstract

Porous silicate materials made by low temperature sol-gel process are promising host matrices for encapsulation of biomolecules. Their mechanical strength, chemical inertness, hydrophilic nature, and above all, their optical transparency makes them an exciting platform for development of biosensors. To date, researchers have focussed on sol-gel routes using alkoxides for encapsulation of biomolecules. However, formation of alcohol as a byproduct is an undesired complication as it can have detrimental effect on the activity of entrapped biomolecules. We have developed a novel sol-gel process to encapsulate biological molecules (such as enzymes, antibodies and cells) that uses neutral pH, room temperature, and does not generate alcohol as a byproduct. The process uses sodium silicate as precursor and is carried out in two steps- preparation of a low pH silicate sol followed by gelation at neutral pH in a buffer containing biomolecules. We developed a novel homogeneous immunoassay for 2,4,6-trinitrotoluene (TNT), and have encapsulated the immunoassay reagents in sol-gel matrices to produce dispersible biosensors for the detection of TNT. Using the sol-gel doped with immunoassay reagents, we can detect TNT at low ppm levels. We also report encapsulation of *E. Coli* cells expressing the enzyme organophosphorous hydrolase (OPH) on the cell surface in sol-gel matrices. The cell-doped sol-gel material can be used to develop biosensors for detection of organophosphates.

Encapsulation of enzymes and cells in sol-gel matrices for biosensor applications
Anup .K. Singh, Alok Gupta, Ashok Mulchandani, Wilfred Chen, Rimple Bhatia, Joseph S. Shoeniger, Carol S. Ashley, and C. Jeffrey Brinker, SPIE 3858 (1999) 10-16.

4. Production of modified enzymes by site-directed mutagenesis

A significant factor that currently limits the sensitivity of the TNT immunoassay discussed above is loss of enzyme activity upon conjugation of analyte molecules to the enzyme. Success of the immunoassay scheme requires that at least one analyte molecule be conjugated very close to the active site of enzyme. G6PDH, fortunately, has a lysine molecule in its active site that can be used for conjugation to analyte. For most enzymes, however, the active site is located in a ‘cleft’or a ‘pocket’ so as to restrict accessibility by molecules other than specific substrates. This means that the lysine in the active site is not readily accessible for conjugation to the analyte. In order to overcome this steric resistance, during conjugation a huge molar excess of analyte molecules must be added to the reaction mixture. This leads to attachment of analyte molecules all over the enzyme, rather than only at the active site. Specifically for the TNT assay case, G6PDH contains approximately 106 lysine molecules. Not unexpectedly, during analyte conjugation, modification of the enzyme at a large number of these sites leads to a significant loss of

enzymatic activity. G6PDH loses activity exponentially as more and more TNT molecules are attached.

One way to avoid this denaturation of enzyme upon conjugation is to minimize the over-labeling by the analyte. Ideally, all one needs for the conjugate to perform successfully in the immunoassay is one analyte molecule conjugated close to the active site. This can be accomplished by employing recombinant DNA technology to introduce a non-native moiety in the vicinity of active site for conjugation to the analyte. This moiety will offer a unique site for chemical modification and hence by choosing the appropriate chemistry, a single analyte molecule will be conjugated to the recombinant enzyme.

In addition to the expected increase in activity of the enzyme conjugate, the ability to control conjugation at a unique position near the active site of the enzyme offers a tremendous potential to adapt the immunoassay strategy to detection of a wide range of analytes, not only TNT. If the position and chemistry of the enzyme conjugation site can be precisely controlled, then it should be possible to selectively conjugate the enzyme with surrogates of any desired analyte for which antibodies can be obtained.

In order to pursue this strategy, our Sandia National Laboratories team initiated a collaboration with researchers at University of California, Riverside, to produce modified enzymes using site-directed mutagenesis.

4.1 Experimental section

Bacteria, Plasmid and Growth Conditions. The *Bacillus subtilis* BRB 1 was kindly provided by Dr. Pauli Kallio. Cloning steps were carried out in *E. coli* JM109 or *E. coli* XL-1 Blue (Stratagene, CA). Plasmid *p*MAL was obtained from New England Biolabs (MA). Bacteria were grown in Luria broth medium supplemented, if necessary, with 100 μg/mL ampicillin, on a rotary shaker with vigorous shaking at 37°C.

DNA Techniques. Preparation of plasmid DNAs, enzyme reactions, and transformation of *E. coli* cells was carried out as described by Maniatis *et al*. (1989).

Enzyme Assay, Protein Determination, and SDS-PAGE. Glucose dehydrogenase activity was determined by spectrophotometric measurements (340nm) of NADH formation at 37°C. The activity assay was performed in 0.35 M Tris-HCl pH 8.0 in the presence of 140 mM D-glucose and 15 mM NAD^+. Protein content was determined by the method of Bradford (1976) using bovine serum albumin as a standard. SDS-PAGE was performed on 12% polyacrylamide slab gels using a Tris-glycine, pH 8.6, discontinuous buffer system as described by Laemmli (1970).

Stability measurements. To stabilize glucose dehydrogenase in both crude cytosolic extract and purified fractions, BSA (1 mg/mL), glycerol (20% v/v), 0.1 M potassium phosphate, 0.1 M NaCl, Zn^{2+}, Ca^{2+}, Mg^{2+}, Mn^{2+} and DTT were tested by incubating the

sample with above mentioned compounds and subsequently assayed for GDH activity. All ions and DTT were added to the final concentration of 1 mM.

Construction and Expression of GDH Gene. Chromosomal DNA of *B. subtilis* BRB 1, isolated by phenol/chloroform extraction, was used as a template DNA for generating the GDH gene. Primers GDH-F1 (5' ggaattccatatgcaccaccaccaccaccacatgtatccggatttaaaagg 3') and GDH-R1 (5' gaattcctgcagttaaccgcggcctgcctggaatga 3') were used during DNA amplification. PCR reaction contained 1 unit of *Taq* DNA polymerase, 50 ng of DNA template, 100 μM each dNTP, and 200 μM of each primer in a total volume of 50 μl. The cycling parameters were 95°C for 1 min, 45°C for 1 min, and 72°C for 2 min for 35 cycles. PCR product was purified by GeneClean Kit II (Bio 101, CA) and digested with *Nde* I and *Pst* I enzymes, respectively. The final DNA product was cloned into the pMAL vector, previously digested with *Nde* I and *Pst* I, to yield the pMAL-GDH vector. Bacteria (*E. coli* strain JM109) were transformed with the pMAL-GDH vector and clones carrying the plasmid were identified through restriction analysis. *E. coli* JM109 carrying pMAL-GDH plasmid were cultured to express the GDH to confirm the presence of glucose dehydrogenase by SDS-PAGE and enzyme assay. Specifically, bacteria were grown in LB medium supplemented with 100 μg/mL ampicillin till the OD (600nm) reached 1.0. Then 1mM IPTG was added to the culture which was harvested after 3 hours by centrifugation (5000 *g*, 4°C, 15 min). The pellet was resuspended in 0.1 M potassium phosphate buffer pH 7.0, sonicated (3x 10 sec) on ice, and the soluble fraction containing GDH resulted as a supernatant after centrifugation (30,000 *g*, 4°C, 20 min).

Computer Analysis. Due to the high similarity of the amino acid sequence of glucose dehydrogenase from *B. subtilis* BRB 1 and glucose dehydrogenase (GCO) from *Bacillus megaterium* that crystal structure has been resolved, RasMol 2.6 (Roger Sayle, Glaxo Wellcome Research and Development) was used for prediction of three amino acids to be substituted by cysteine residue.

PCR-Based Site-Directed Mutagenesis. The technique based on QuikChange™ Site-Directed Mutageneis Kit (Stratagene, CA) was employed to produce cysteine containing mutants. Primers used in PCR are summarized in Table1. PCR reaction contained 2.5 unit of *PfuTurbo* DNA polymerase, 50ng of DNA template, 250uM each dNTP, and 100 nmol of each primer in a total volume of 50 μl. The DNA was denatured at 95°C for 30 seconds, which was followed by 16 cycles of 95°C for 30 seconds, 55°C for 1 minute, and 68°C for 14 min. 10 μl of PCR reaction was digested with *Dpn* I for 2 hrs at 37°C, consequently, *E. coli* XL-1 Blue supercompetent cells were transformed with 1 μl of *Dpn* I reaction mixture. Transformants were screened by plasmid restriction analysis.

Purification of GDH. Glucose dehydrogenase was purified on His Bind Quick Columns (Novagen, Medison, WI) . The column was equilibrated with 25 ml of Buffer A (40 mM Tris-HCl pH 7.9 containing 0.5 M NaCl), then 2 ml of crude cytosolic extract was applied followed by 45 ml of equilibrating Buffer A. The bound proteins were eluted by stepwise gradient (20 ml each) of 10, 25 and 100 mM EDTA in Buffer A. 10 ml fractions were collected and assayed for GDH activity. The purification was also monitored by SDS-PAGE.

Desalting and Buffer Exchange. For desalting and buffer exchange prepacked PD-10 columns (Amersham Pharmacia Biotech) were used.

Sequencing. Sequencing of obtained clones was performed with primers 21M13 (5' TGTAAAACGACGGCCAGT 3') and C2XUF (5' GGAAACAGCCAGTCCGTTTAG 3') at Loma Linda University (CA).

4.2 Results

Bacillus subtilis is known to contain NAD^+-dependent glucose dehydrogenase (Lampel *et al.* (1986) that does not contain any cysteine residue. Chromosomal DNA from *B. subtilis* BRB 1 served as a template for PCR amplification of *gdh* gene. During amplification *Nde I* and *Pst I* sites were introduced to the ends of the gene for cloning into pMAL vector. For subsequent purification hexa histidine tail was also added to the N-terminal sequence of the *gdh* gene. Transformants containing pMAL-GDH plasmid were tested for the presence of GDH activity in soluble fraction of *E. coli* JM109/pMAL-GDH. Recombinant GDH was found to be both NAD^+ and $NADP^+$-dependent, exhibiting higher affinity to NAD^+. The size of the enzyme subunit was found to be 31,000 as revealed by SDS-PAGE. The presence of hexa histidine tail was confirmed as the enzyme was successfully bound on Ni-NTA agarose resin (QIAGEN, Valencia, CA). Among the tested stabilizing agents 0.1 M potassium phosphate buffer pH 7.0 exhibited the best stabilizing properties at both tested temperatures (4°C and –20°C), therefore all enzyme preparations were prepared and store in above mentioned buffer system.

The nucleotide sequence of clones GDH1 and GDH2 shown in Fig. 1. Indicates high similarity to all listed GDHs from *Bacillus* species. Due to its high homology prediction of amino acids to be present close to the active site of the enzyme and also on the surface, were performed on GCO from *B. megaterium*. The crystal structure of GCO showed Asp44, Ile195 and Met212 to be suitable candidates for cysteine substitution, fulfilling both above mentioned conditions.

In vitro site-directed mutagenesis as an invaluable technique for introducing a single amino acid substitution into known protein structure. Point mutation performed by *PfuTurbo* DNA polymerase enables high efficiency of such mutation, and furthermore, enables fast procedure with decreased potential for generating random mutations during the mutagenesis. Three mutants have been prepared, in all cases cysteine residue was introduced into previously cloned GDH. For the gene amplification plasmid DNA from the clone GDH1 was used. For the future work following mutant clones were chosen, for D44C (Asp44→Cys44), M212C (Met212→Cys212) and I195C (Ile195→Cys195) mutations clones D44C-6, M212C-11 and I195C-11, respectively. As revealed by sequencing analysis in all three mutant variants (D44C-6, M212C-11 and I195C-11) targeted amino acid was successfully mutated to cysteine residue.

For subsequent TNT-analogue binding wild type as well as three mutants were purified using its hexa histidine tail on His Bind Quick Columns. In all cases the GDH was eluted during 0.25 mM – 1 M EDTA elution. The specific activities of purified

enzyme preparations are summarized in Table 2. The results clearly indicate that D44C-6 variant has the highest specific activity, which is the same as the wild type, thus mutation of Asp44 did not have any significant effect on enzyme activity. On the other hand, variant I195C-11 has only one third of the wild type activity, therefore in this case incorporating cysteine residue led into conformation changes that restrict substrate or cofactor binding. Availability of three mutant GDHs serves as a good starting point for TNT-analogue binding experiments. All purified enzyme preparations from D44C-6, M212C-11 and I195C-11 were successfully dialysed using PD-10 to remove small molecular weight components that could subsequently prevent TNT-analogue coupling.

These purified enzyme preparations are now available for conjugation with trinitrobenzenesulfonic acid, and will be tested for effectiveness in the TNT immunoassay described in the preceding sections.

4.3 References

Bradford, M M; 1976, Anal Biochem 72, 248 –254
Laemmli, U K; 1970, Nature 227, 680-685
Lampel, K A; Uratani, B; Chaudhry, G R; Ramaley, R F; Rudikoff, S; 1986, J. Bacteriol 166, 238-243
Sambrook, J; Fritsch, E F; Maniatis, T; Molecular Cloning: A Laboratory Manual 2nd ed; Cold Spring Harbor Laboratory Press, NY, 1989

5. Signal-to-noise ratio (SNR) estimates for field fluorescence measurements.

Our primary goal has been to develop distributable sensor particles that can detect trace chemical target species by reaction to form a fluorescent signature. However, we have also evaluated several operational scenarios for use of these materials. Specifically, we have developed a simplified but flexible spreadsheet-based model to estimate the spectral signal to noise ratio for fluorescence interrogation of the sensor particles as a function of several parameters including particle coverage, sensor standoff range, and integration time. Further, the estimates provided by these calculations have been compared to a limited number of field tests performed using Sandia's stationary uv-visible fluorescence LIDAR. These results demonstrate that the sensor particles will provide useful signals in non-imaging chemical detection applications at intermediate (~kilometers) standoff range.

The initial concept for employment of the sensor particles was airborne standoff detection using a UAV-based fluorescence measurement system. Therefore, the first versions of the spreadsheet SNR estimator were set up for range estimates on the order of a kilometer. Two versions were investigated: An imaging type where the goal was to estimate the SNR for individual pixels of a spatial image of fluorescence intensity vs. x,y position in a target plane, and a nonimaging type where the goal was evaluation of spectral SNR for a spatially averaged measurement of fluorescence intensity vs. emission

wavelength. In the latter case, fluorescence intensity is integrated from a single relatively large area in the target plane. For both cases, commercial off the shelf (COTS) hardware was assumed for both the fluorescence excitation laser and focal plane array detector.

For the case of the imaging sensor, the focal length and aperture of the collecting optics were variable parameters, thus determining the transverse magnification of the collector. The desired spatial resolution of the image was set as a projected pixel dimension at the target plane. If the physical size of the focal plane array (charge coupled device – CCD) pixels was smaller than the projected image of the desired target pixels, signals from multiple CCD pixels were binned in the SNR calculations. Spectral resolution of the imaging system was determined in the calculations by the use of appropriate narrow-bandpass optical filters.

For the case of the nonimaging, spectrally resolving detector, the divergence angles of the excitation laser beam and collection telescope were used as adjustable parameters along with the standoff range to determine the size of the target area illuminated and interrogated. Upper and lower spectral wavelengths were entered, and the spectral window width combined with grating dispersion and physical pixel size were used to estimate number of pixels binned per resolution interval in the collected spectrum. The field measurements described below were made with this type of detection system.

Note that for both the imaging and nonimaging systems, no attempt was made to model aberrations or estimate an optical point spread function for the collection optics. Thus, the SNR calculations were considerably simplified. The results should therefore be considered useful as order of magnitude estimates rather than attempts at precise predictions. The goal was to determine if various operational concepts for employment of the particle sensors are physically reasonable.

The SNR was estimated according to the equation

$$SNR = MPQ_e t/\{(P+B)MQ_e t+MDt+N_r^2+N_{AD}^2\}^{1/2} \qquad [1]$$

Where

- M = number of pixels binned = f(physical dimensions, magnification, range)
- P = number of signal photons per second per pixel, the *SIGNAL*
- Q_e = quantum efficiency of detector. Contains multiple factors for ICCD. Values obtained from detector manufacturer's specifications
- t = time = receiver gate time X number of pulses (duty cycle)
- B = background photons per second per pixel, estimated from reflectance and atmospheric scatter
- D = detector dark current per pixel per second. Manufacturer's specification
- N_r = RMS noise from CCD readout amplifier. Manufacturer's specification

– N_{AD} = analog to digital converter RMS noise. Manufacturer's specification

Calculations were performed using manufacturer's specifications for CCD detectors with and without image intensifier tubes. For the intensified CCD arrays (ICCD) the additional complexity of the device is accounted for by changes in the overall quantum efficiency of the detector vs. wavelength and by the dark current and noise factors. Representative input parameters used for SNR estimates for the imaging and nonimaging systems are summarized in Tables 1 and 2, respectively. The key difference in these systems is that the nonimaging system effectively integrates fluorescence returns over a much larger area than the small pixels of an imaging system, leading to greatly enhanced SNR values.

TABLE 5.1: Representative Parameters for a Fluorescence Imaging System

INPUT PARAMETER	VALUE	REMARKS
Fluorescence photon wavelength, nm	460	Prototype sensor particle output wavelength
Pump laser photon wavelength, nm	355	Nd:YAG 3rd harmonic, used to pump prototype particles
Pump laser pulse width, ns	30	COTS hardware
Pump laser output energy per pulse, J	0.03	COTS hardware
Pump laser rep rate, Hz	10	COTS hardware
Target range, m	1000	UAV standoff estimate
Diameter of area to be imaged per shot, m	50	Target area estimate per image
Required pixel dimension (resolution) at target plane, m	0.05	Target resolution
Actual pixel dimension at detector plane, m	9.00E-06	COTS hardware
Number of pixels across array	1024	COTS hardware
Receiver aperture radius (m)	0.15	UAV-compatible estimate
Receiver gate time (s)	4.00E-07	COTS hardware
Optical transmission of system	0.3	Telescope/detector throughput
Spectral bandwidth, nm	10	Filter bandwidth
Receiver optics, f number	3	Determines transverse magnification, therefore pixel binning vs. range
Atmospheric attenuation at laser wavelength, 1/m	3.00E-04	Clear air value, reasonable at short range for uv-vis
Atmospheric attenuation at emission wavelength, 1/m	3.00E-04	
Particle diameter, m	2.54E-04	Prototype particles 100-300 mesh sizes
Particle density, g/cm^3	1	Prototype particle density
Total mass of particles distributed, kg	100	Particle coverage 1 mg/cm2, based on lab measurements of particle brightness vs. field requirements for mass distribution of sensor material
Edge dimension of square target field, m	100	
Average fluorescence efficiency of	0.1	Estimated from lab spectral

single particle		measurements
Quantum efficiency of CCD at fluorescence wavelength	0.12	COTS value for CCD w/o image intensifier tube. Additional gain factors included for intensified array.
Approximate solar irradiance at 460 nm, W/cm^2-sr-nm	4.45E-06	US Air Force PLEXUS model
Lambertian reflectance of target area at 460 nm	0.2	Approximate value for soil
Number of shots integrated	1	Multiple shots increase SNR but require precise optical pointing and tracking
CCD dark current, electrons per pixel per second	0.05	COTS hardware values
CCD read noise, electrons rms per pixel	12	COTS hardware values

TABLE 5.2: Representative Parameters for a Non-Imaging System

INPUT PARAMETER	VALUE	REMARKS
Fluorescence photon wavelength, nm	460	Prototype sensor particle output wavelength
Fluorescence "square wave bandwidth", nm	10	Sufficient for resolution of multiple emission peaks
Fluorescent dye total Q.E.	0.8	Lab measurement of dye(s)
Fraction of total dye fluorescence within square wave	0.43	Lab spectral measurement
Effective QE within square wave bandwidth	0.344	Calculated from bandwidth and lab spectral measurement
Pump laser photon wavelength, nm	355	Nd:YAG 3rd harmonic, used to pump prototype particles
Pump laser pulse width, ns	10	COTS hardware
Pump laser output energy per pulse, J	0.03	COTS hardware
Pump laser rep rate, Hz	30	COTS hardware
Target range, m	1000	UAV standoff estimate
Pump beam divergence, microrad	500	UAV hardware value
Diameter of area illuminated, m	0.5	Calculated from range and divergence. Note<<Image area
Collection telescope divergence, microrad	850	UAV hardware value
Actual pixel dimension at detector plane, m	26 microns	COTS hardware value for ICCD
Receiver aperture radius (m)	0.15	UAV hardware value
Receiver gate time (s)	4.00E-7	COTS hardware value
Optical transmission of system	0.25	UAV hardware value
Spectrum upper wavelength limit, nm	700	UAV hardware value
Spectrum lower wavelength limit, nm	300	UAV hardware value
CCD array width, pixels	1024	COTS hardware value
CCD array height, pixels	256	COTS hardware value
Approximate grating dispersion, nm per pixel	0.390625	COTS hardware value
Atmospheric attenuation at laser wavelength, 1/m	3.00E-04	Clear air value, reasonable at short range for uv-vis
Atmospheric attenuation at emission wavelength, 1/m	3.00E-04	
Particle diameter (100 mesh), m	2.54E-04	Prototype particle size estimate
Particle density, g/cm^3	1	Prototype particle density
Total mass of particles distributed, kg	100	Same density as assumed for imaging case
Edge dimension of square target field, m	100	
Molar concentration of dye in particles, mole/lit	1.61E-04	Lab measurement
Molar extinction coeff of dye, lit/mole-cm	5.00E+04	Lab measurement
Average fluorescence efficiency of single particle	6.37E-02	Calculated from Beer-Lambert absorption and dye QE
Photocathode Quantum efficiency	0.15	COTS hardware value
Intensifier gain (CCD counts per photoelectron)	124	COTS hardware value

Continued on next page

Table 5.2: Continued from preceding page		
Approximate solar irradiance at 460 nm, W/cm^2-sr-nm	4.45E-06	US Air Force PLEXUS model
Lambertian reflectance of target area at 460 nm	0.2	Approximate value for soil
Equivalent background illumination (noise from ICCD photocathode), count/pixel/sec	0.052	COTS hardware value
CCD dark current, counts/pix/sec	3.00E+01	COTS hardware value
CCD readout noise, rms counts/pixel	4.50E+00	COTS hardware value
Number of shots integrated	1-1000	Pointing not as critical for non-imaging system
Controller noise, A/D counts	0.51	COTS hardware value

5.1 Representative results: Fluorescence SNR vs. standoff range

Calculated values of SNR vs. standoff range are displayed in Figure 5.1 for a notional imaging system and field coverage of the chemical sensor particles as described by the parameters summarized in Table 5.1.

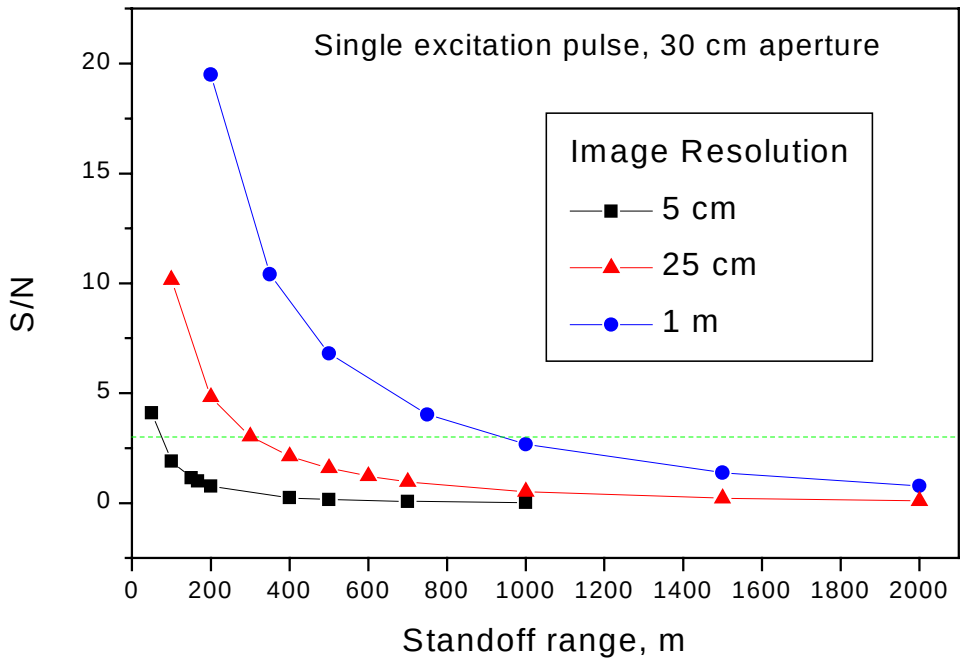

Figure 5.1: SNR vs. Range for a fluorescence imaging system

The SNR has been estimated for three different values of image resolution. The dashed line is set at SNR=3, a qualitative estimate of the required SNR for useful

interpretation of images. These estimates are based on acquiring an image from a 50 m wide target area with a single laser excitation pulse, using a 30 cm diameter collection telescope and a COTS CCD detector. At high resolution, useful signal is obtained only at short range. The effect of integrating signal over multiple laser excitation pulses is summarized in Figure 5.2 for imaging a 50 meter diameter target area.

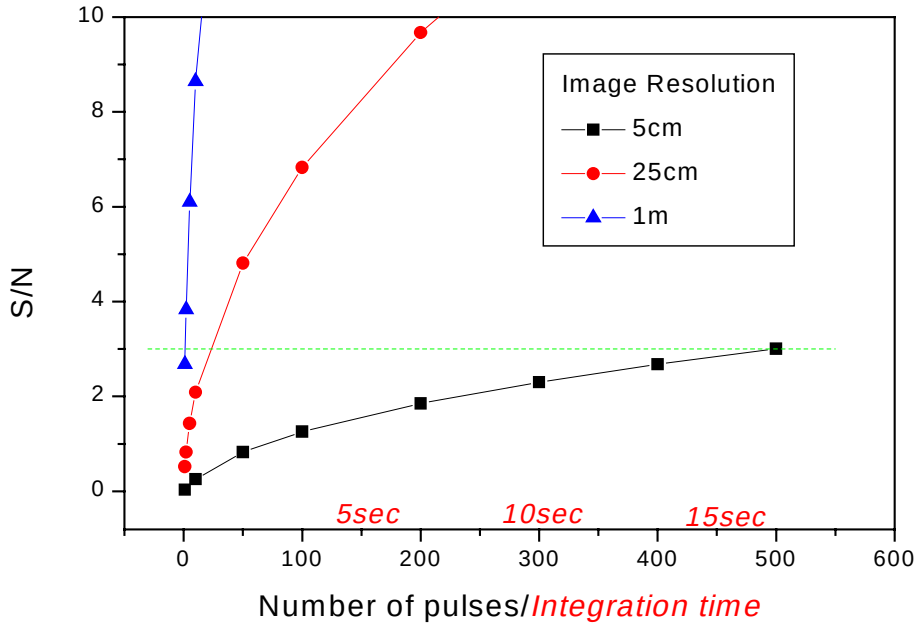

Figure 5.2: Estimated Signal to Noise vs. Pulse Integration at 1 km

It is apparent that integrating for a modest amount of time could result in useful SNR for an imaging system. However, in order to accomplish this, the pointing and tracking requirements on an airborne (moving) optical sensing platform are severe. As an example, a 5 cm target area pixel dimension implies a pointing accuracy of 5 microradians at 1 km standoff range. Targeting and holding the optical system within 5 microradians for 20 seconds from a moving platform is within the realm of current gimbal and tracking technology, but would require a significant investment in engineering resources. A stationary optical measurement platform would have less severe requirements, although refraction effects in the atmosphere near the ground could still potentially cause degradation of the calculated pixel resolution.

A series of signal to noise estimates vs. standoff range for a spectrally resolved, but spatially unresolved (non-imaging) fluorescence detection system is displayed in Figure 5.3. This system uses a nominal beam divergence of 500 microradians and a telescope divergence of 850 microradians, in order to lessen requirements for pointing accuracy of the pump laser. Thus, at a 1 km standoff range, the system would illuminate only a small area (~0.5 m diameter) using the total output pulse energy of the excitation laser. Presuming that the photobleaching limit is not reached, the total integrated fluorescence signal from that area would be much greater than the fluorescence signal

acquired from a single pixel of comparable size in the imaging system. The SNR is calculated for a spectral interval of 10 nm, centered at 460 nm. This wavelength interval was chosen because it matches the emission characteristics of our prototype chemical sensor particles.

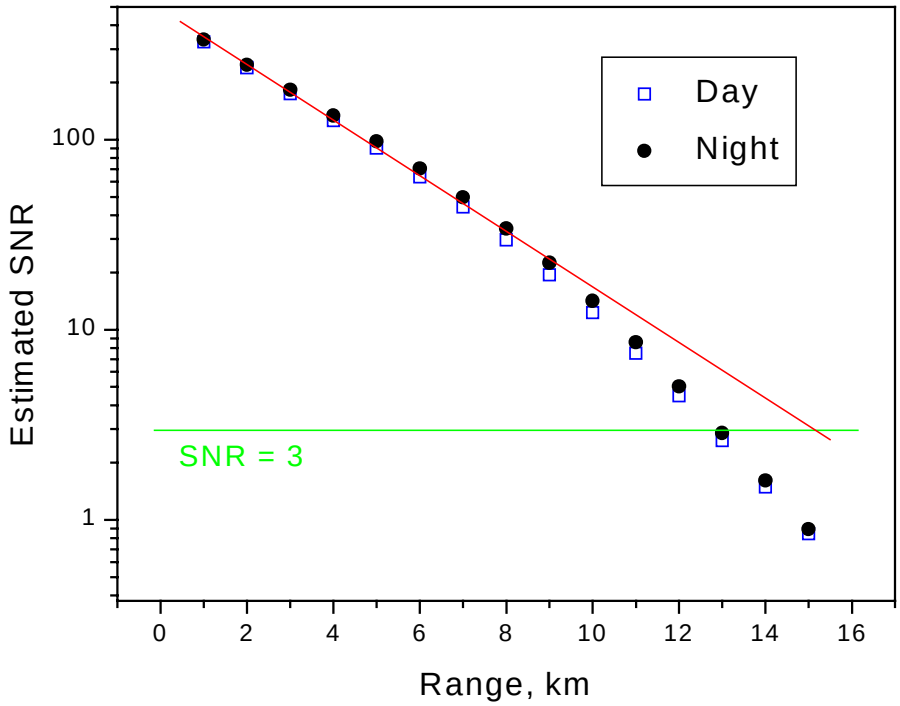

Figure 5.3: Estimated Signal to Noise vs. Range for Non-imaging detector

The estimated SNR is on the order of 200 at 1-2 kilometers range for the notional non-imaging system, indicating that measurements of this type should be practical. Another point to note from the estimates summarized in Figure 5.2 is that the background scattered light is underestimated in the calculations, since the SNR figures for day (sunlight background) and night operation differ only slightly. Improved radiance values, estimated using the US Air Force PLEXUS software package, increased the difference in the day and night estimates only slightly. Therefore, the SNR estimation spreadsheet would benefit from further modifications to improve the estimate of daylight background effects.

5.2 Comparison of SNR estimates with field measurements

To date, our LDRD project has been primarily concerned with the detection of trace concentrations of nitroaromatic explosives, e.g., TNT, for landmine detection applications. We have produced prototype chemical sensor particles that produce a change in their fluorescence spectral signature upon exposure to TNT. We have used these materials in conjunction with a uv-visible fluorescence LIDAR system, built by

Sandia in support of DOE programs, in order to test the SNR estimates discussed above. Briefly, we prepared a series of 2-inch diameter targets consisting of natural soils with and without TNT spikes. The prototype sensor particles were sprinkled onto the soil targets at an average coverage on the order of 1 mg particles per square centimeter. After wetting with HPLC grade water (to facilitate transport of the TNT signature molecules in the soil) the targets were allowed to dry ~24 hours. Fluorescence spectra were then acquired from the 2-inch targets at 500 m standoff range, using 355 nm excitation pulses. A representative spectrum from this experiment is displayed in Figure 5.4.

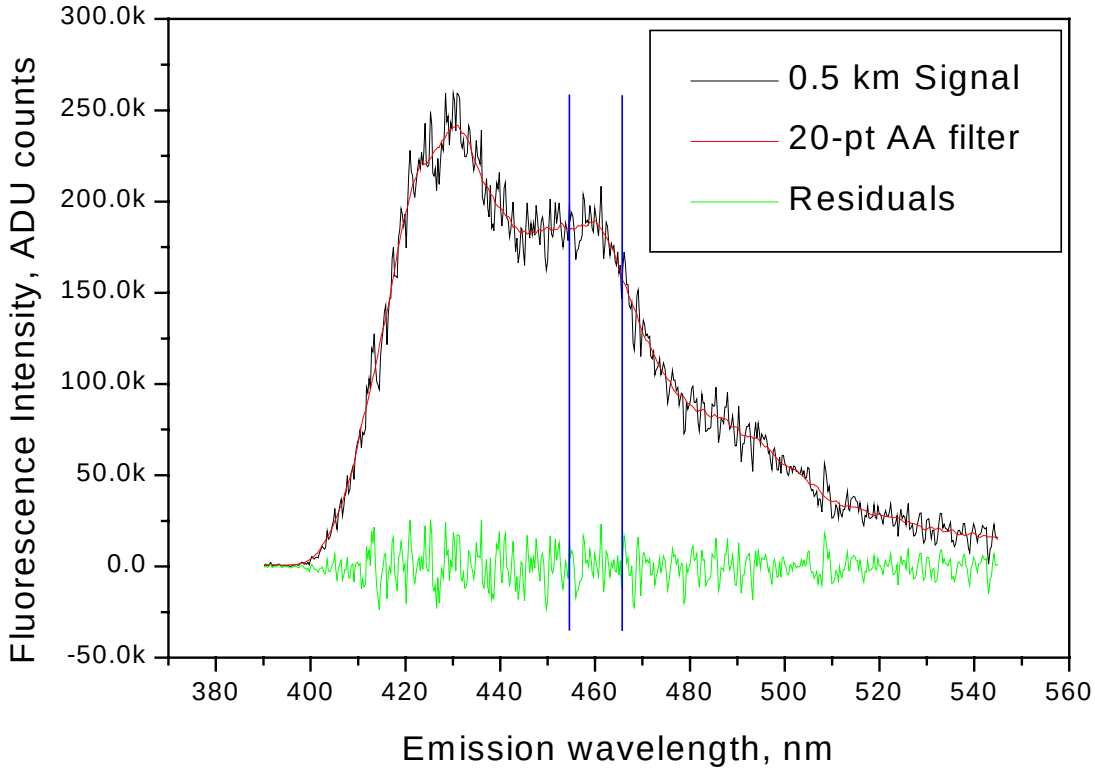

Figure 5.4: Fluorescence spectrum of sensor particles acquired at 500 m.

The signal to noise ratio was estimated for this spectrum in a 10 nm bandpass region around one of the particle emission peaks. The integrated SNR value was 215. The SNR was also estimated for this experiment using the spreadsheet model discussed above. The non-imaging model was used, with modifications of the parameters listed in Table 5.2. The parameter values (target area, telescope aperture, ICCD gain, laser power, integration time) were adjusted in the spreadsheet to match the actual values measured for the field LIDAR system. The estimated SNR result was 278, in good agreement with the result measured from the spectrum. Thus, although there are a number of known approximations in the spreadsheet, we are confident that the values generated by the model are of the correct order of magnitude.

The SNR estimates are in reasonable agreement with the limited field test data available, indicating that the estimates can be relied on to give order-of-magnitude scale predictions of system performance vs. operational parameters. Further, these estimates and field tests provide confidence that the fluorescent distributed sensor particles discussed in this report can be spectrally detected with available optical hardware.

6. Remote detection of explosives in soil by TNT-induced quenching of polymeric fluorescent particles.

Abstract

Environmental fate and transport studies of explosives in soil indicate that 2,4,6-trinitrotoluene (TNT) and similar products such as dinitrotoluene (DNT) are major contributors to the trace chemical signature emanating from buried landmines. Chemical analysis methods are under development that have great potential to detect mines, or to rapidly classify electromagnetically detected anomalies as mines vs. "mine-like objects". However, these chemical methods are currently confined to point sensors. In contrast, we have developed a method that can ***remotely*** determine the presence of nitroaromatic explosives in surface soil. This method utilizes a novel distributed granular sensor approach in combination with uv-visible fluorescence LIDAR (Light Detection and Ranging) technology. We have produced prototype sensor particles that combine sample preconcentration, explosives sensing, signal amplification, and optical signal output functions. These particles can be sprayed onto soil areas that are suspected of explosives contamination. By design, the fluorescence emission spectrum of the distributed particles is strongly affected by absorption of nitroaromatic explosives from the surrounding environment. Using ~1mg/cm^2 coverage of the sensor particles on natural soil, we have observed significant spectral changes due to TNT concentrations in the ppm range (μg TNT/g soil) on 2-inch diameter targets at a standoff distance of 0.5 km. These field measurements have also been used to validate calculations of fluorescent signal/noise for the granular sensor particles as a function of several variables, including particle and receiver characteristics, standoff range, pump laser characteristics, and particle coverage. Some implications of these measurements and calculations for field deployment of the sensor particles are discussed.

Remote Detection of Nitroaromatic Explosives in Soil using Distributed Sensor Particles, R. Joseph. Simonson, Bradley G. Hance, Randal L Schmitt, Mark S. Johnson, and Philip J. Hargas, SPIE 4394 (2001) 879

7. Conclusions

Remote detection of trace chemical compounds can be accomplished by distributing sensor particles whose fluorescence is affected by reaction with the target analytes. We have demonstrated two examples of this chemical-to-fluorescence signal transduction strategy.

The first strategy relies on the use of an aqueous sol-gel synthesis route to produce porous silica particles that can immobilize biomolecules, enabling the use of an enzyme-amplified immunoassay in a distributable host matrix. We have demonstrated that enzymatic activity can be maintained in such hosts for useful periods (weeks). We have also successfully demonstrated in the laboratory an enzyme-amplified substitutional immunoassay for TNT in a porous silica matrix. Further, we have prepared modified enzymes with artificially induced conjugation sites near the catalytic site of the enzyme. This strategy allows for the potential modification of the immunoassay by conjugating a wide variety of target molecules to the enzyme. If such modification is successful, then the immunoassay strategy could be adapted for detection of almost any molecule for which antibodies can be obtained.

The second transduction strategy we investigated is based on TNT-induced quenching of a fluorescent polymer. By formulating sensor particles that combine the sensing polymer with a preconcentrating matrix and an internal fluorescence emission standard dye, we have successfully detected 1 ppm TNT in natural soil at a standoff range of 0.5 km. This demonstrates the feasibility of our fluorescence-based remote chemical detection strategy. This method has been selected by the U.S. Army (Night Vision Laboratory) for limited scale field testing for the detection of buried land mines. The quenching-based detection strategy shows promise for specific classes of target materials, and is relatively easy to implement as compared with the bio-inorganic immunoassay approach. However, the quenching transduction mechanism is not as readily adaptable to a broad range of target compounds as the immunoassay approach.

Distribution

1 Ashok Mulchandani
Dept. of Chemical and Environmental Engineering
University of California
Riverside, CA 92521

1 Wilfred Chen
Dept. of Chemical and Environmental Engineering
University of California
Riverside, CA 92521

1 Rimple Bhatia
Superior MicroPowders
3740 Hawkins NE
Albuquerque, NM 87109

1	MS0806	Bradley G. Hance
6	MS0892	R. Joseph Simonson
1	MS1349	Carol S. Ashley
6	MS1349	C. Jeffrey Brinker
1	MS1423	Philip J. Hargis, Jr.
1	MS1423	Mark S. Johnson
1	MS1423	Randal L. Schmitt
1	MS9951	Joseph S. Schoeniger
6	MS9951	Anup K. Singh

1	MS0899	Central Technical Files, 8945-1
2	MS0899	Technical Library, 9616
1	MS0612	Review and Approval Desk, 9612, for DOE/OSTI
1	MS0161	Patent and Licensing, 11500
1	MS0188	LDRD Program Office, 1030